Optomechanical dynamics in the $\mathcal{PT}$- and broken-$\mathcal{PT}$-symmetric regimes

Hai Xu,[1] Deng-Gao Lai,[2,*] Yi-Bing Qian,[1] Bang-Pin Hou,[1,†] Adam Miranowicz,[2,3] and Franco Nori[2,4,5]

[1]*College of Physics and Electronic Engineering, Institute of Solid State Physics, Sichuan Normal University, Chengdu 610101, People's Republic of China*

[2]*Theoretical Quantum Physics Laboratory, RIKEN Cluster for Pioneering Research, Wako-shi, Saitama 351-0198, Japan*

[3]*Institute of Spintronics and Quantum Information, Faculty of Physics, Adam Mickiewicz University, 61-614 Poznań, Poland*

[4]*RIKEN Center for Quantum Computing (RQC), 2-1 Hirosawa, Wako-shi, Saitama 351-0198, Japan*

[5]*Physics Department, The University of Michigan, Ann Arbor, Michigan 48109-1040, USA*

(Received 18 July 2021; revised 3 November 2021; accepted 4 November 2021; published 17 November 2021)

We theoretically study the dynamics of an optomechanical system, consisting of a passive optical mode and an active mechanical mode, in the $\mathcal{PT}$- and broken-$\mathcal{PT}$-symmetric regimes. By fully analytical treatments for the dynamics of the average displacement and particle numbers, we reveal the phase diagram under different conditions and the various regimes of both $\mathcal{PT}$ symmetry and stability of the system. We find that by appropriately tuning either mechanical gain or optomechanical coupling, both phase transitions of the $\mathcal{PT}$ symmetry and stability of the system can be flexibly controlled. As a result, the dynamical behaviors of the average displacement, photons, and phonons are radically changed in different regimes. The presented physical mechanism is general and this method can be extended to a general model of dissipative and amplified coupled systems. Our study shows that $\mathcal{PT}$-symmetric optomechanical devices can serve as a powerful tool for the manipulation of mechanical motion, photons, and phonons.

DOI: 10.1103/PhysRevA.104.053518

I. INTRODUCTION

Cavity optomechanics, which explores the radiation-pressure interaction between electromagnetic and mechanical systems, has attracted considerable attention both theoretically and experimentally in the past decades [1–3]. Due to optomechanical interaction, many interesting phenomena have been shown, such as cooling of mechanical oscillators to their quantum ground states [4–16], photon blockade [17–25], generation and transfer of squeezed light [26–30], measurements with a high precision within the standard quantum limit [31–33], optomechanically induced effects of nonreciprocity [34–37], transparency (OMIT) [38–42], absorption (OMIA) [43], and amplification [44,45].

It is usually assumed in quantum mechanics that the Hamiltonian must be Hermitian in order to ensure that their eigenvalues are real and that the time evolution operator is unitary. However, for parity-time ($\mathcal{PT}$)-symmetry quantum mechanics [46–48], the effective Hamiltonian of a quantum system can be non-Hermitian, which is useful to describe a quantum system interacting with its environment. Note that this generalized approach to quantum mechanics does not lead to any violations of no-go theorems in standard quantum mechanics, including quantum information [49]. A phase transition from the $\mathcal{PT}$-symmetric regime to the broken-$\mathcal{PT}$-symmetric regime can occur, when the $\mathcal{PT}$-symmetric condition is broken, and some eigenvalues become complex [50,51]. The phase transition between the two regimes has been observed experimentally using various gain-loss-balanced systems, such as $\mathcal{PT}$-symmetric waveguides [52,53], active LRC circuits [54], and $\mathcal{PT}$-symmetric whispering-gallery microcavities [55].

As an emerging frontier, optical-$\mathcal{PT}$-symmetric optomechanical systems [56–64], which are realized by coupling an active (gain) cavity to a passive (lossy) optomechanical cavity, have led to various unconventional phenomena, such as phonon lasers [56,65,66], $\mathcal{PT}$-enhanced OMIT [67–69], $\mathcal{PT}$-induced amplification [70], and coherent perfect absorption [71–73]. Compared to these steady-state behaviors of $\mathcal{PT}$-symmetric systems, their dynamics can provide a more versatile description of these systems.

So far, the dynamics of photons have been predicted in optical-$\mathcal{PT}$-symmetric systems consisting of two waveguides [74] or two coupled cavities [75,76]. Subsequently, the dynamical behavior of the mechanical resonators has been studied in mechanical-$\mathcal{PT}$-symmetric four-mode hybrid optomechanical systems [77]. Despite these advances, the dynamics of a typical optomechanical system, consisting of a passive optical mode coupled to an active mechanical mode, in the $\mathcal{PT}$- and broken-$\mathcal{PT}$-symmetric regimes, and the phase diagram under different conditions, have not yet been revealed.

In this paper, we focus on a *comparative study* of the dynamics of a typical optomechanical system, which consists of a passive optical mode and an active mechanical mode implemented by a mechanical gain, in the $\mathcal{PT}$- and broken-$\mathcal{PT}$-symmetric regimes. Note that the mechanical gain can be achieved by phonon lasing or by coupling the

*denggaolai@foxmail.com
†bphou@sicnu.edu.cn

mechanical mode to another cavity mode driven with a blue-detuned driving field [51,78]. In contrast to previous work [77] investigating the dynamics of mechanical modes in four-mode hybrid optomechanical systems, the aim here is not only to study the dynamics of *both optical and mechanical* modes by *fully analytical* treatments in *typical* optomechanical systems which have more fundamental properties, but also to reveal in detail the *phase diagram* under different conditions.

We find that by appropriately adjusting either the effective optomechanical coupling or the mechanical gain, phase transitions can be clearly observed. We obtain the *phase diagram* under different conditions and the *various regimes* of both $\mathcal{PT}$ symmetry and stability of the system. Using our *exact analytical solutions* of the average displacement and particle numbers, their dynamical behaviors in different regimes can be understood adequately. We find that the energy exchange between the cavity and the mechanical oscillator is rapid (slow) for the $\mathcal{PT}$ (broken-$\mathcal{PT}$)-symmetric regime. This opens up the prospect to manipulate the exchange velocity of the excitations using $\mathcal{PT}$-symmetric optomechanical systems.

Moreover, spontaneous generation of the number of particles is discussed not only when gain compensates loss, but also when gain is *not* equal to loss. Finally, we also find that (i) the average displacement and the average particle numbers *approach their steady-state values* in the asymptotically stable regime, (ii) they increase *exponentially* in the unstable regime, and (iii) the average displacement *oscillates periodically* in the finite-time stable regime, but not asymptotically stable. Our study reveals that $\mathcal{PT}$-symmetric systems can be used for the control of mechanical motion, photons, and phonons. Our method is universal and can be generalized to study the related dynamics in a general model of coupled systems (e.g., two oscillators or waveguides) with loss and gain.

The remainder of the paper is organized as follows: In Sec. II we obtain the master equation of the $\mathcal{PT}$-symmetric-like optomechanical system by using a linearization procedure, when the dissipation and gain rates of the system are phenomenologically considered, and the differential equations for the average values are obtained from the master equation. In Sec. III, the $\mathcal{PT}$ symmetry and stability of the $\mathcal{PT}$-symmetric-like optomechanical system are investigated through a phase diagram. In Sec. IV, the dynamics of the average displacement of the mechanical oscillator are investigated in different regimes for the $\mathcal{PT}$-symmetric-like optomechanical system. And the dynamics of the average particle numbers in different stability regimes for the system are considered in Sec. V. The effect of spontaneous generation of particles is also studied in this section. In Sec. VI, we discuss an extension of the present method to a general gain-loss model, and an experimental realization of our system. Conclusions are presented in Sec. VII. Two Appendixes include the detailed calculations.

II. MODEL AND EQUATIONS OF MOTION OF AVERAGE VALUES

As schematically shown in Fig. 1, the considered optomechanical system consists of a passive cavity (with a loss rate κ) and an active mechanical oscillator (with a mechanical gain rate γ), which is called the $\mathcal{PT}$-symmetric-like optomechanical system [51]. The cavity is driven by a control field with amplitude $\Omega_L = \sqrt{P_L\kappa/\hbar\omega_L}$, in which the input power and the frequency of the control field are given by P_L and ω_L, respectively.

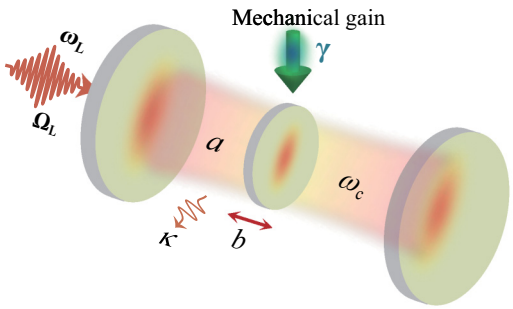

FIG. 1. Schematic of the $\mathcal{PT}$-symmetric-like optomechanical system, which consists of a passive cavity (with photon operator a, loss rate κ, and resonant frequency ω_c), and an active mechanical oscillator (with phonon operator b, mechanical gain strength γ, and resonant frequency ω_m). The cavity is driven by a control field with frequency ω_L and amplitude Ω_L.

The Hamiltonian of the system in the rotating reference frame at the frequency ω_L of the control field reads

$$\hat{H} = \hbar\Delta_c\hat{a}^\dagger\hat{a} + \hbar\omega_m\hat{b}^\dagger\hat{b} - \hbar g\hat{a}^\dagger\hat{a}(\hat{b}+\hat{b}^\dagger) + i\hbar\Omega_L(\hat{a}^\dagger - \hat{a}), \tag{1}$$

where $\hat{a}$ ($\hat{a}^\dagger$) and $\hat{b}$ ($\hat{b}^\dagger$) are the annihilation (creation) operators of the cavity field and the mechanical oscillator, respectively; ω_m is the resonance frequency of the mechanical oscillator, and g is the single-photon optomechanical coupling strength. Moreover, $\Delta_c = \omega_c - \omega_L$ is the detuning between the cavity field of frequency ω_c and the control field of frequency ω_L.

Due to the fact that the control field driving the cavity is strong, the Hamiltonian can be linearized by neglecting higher-order terms. Under the rotating-wave approximation (RWA), the linearized Hamiltonian is given by

$$\hat{H}_{\rm lin} = \hbar\Delta\hat{a}^\dagger\hat{a} + \hbar\omega_m\hat{b}^\dagger\hat{b} - \hbar G(\hat{a}^\dagger\hat{b} + \hat{a}\hat{b}^\dagger), \tag{2}$$

where $\Delta = \Delta_c - g(\beta_s + \beta_s^*)$ is the effective detuning between the cavity field and the control field, and $G = g\alpha_s$ is the effective optomechanical strength, and α_s and β_s are the steady-state solutions of the system given by

$$\alpha_s = \frac{\Omega_L}{i\Delta + \kappa} \text{ and } \beta_s = \frac{ig\alpha_s^*\alpha_s}{i\omega_m - \gamma}. \tag{3}$$

The dynamics of the system, including the loss of cavity field and the gain of the mechanical resonator, can be described by the master equation in the Lindblad form, which is given by

$$\frac{d}{dt}\rho = \frac{1}{i\hbar}[H_{\rm lin}, \rho] + \kappa(2a\rho a^\dagger - a^\dagger a\rho - \rho a^\dagger a) + \gamma(2b^\dagger\rho b - bb^\dagger\rho - \rho bb^\dagger). \tag{4}$$

The equations of motion of the mean values of an operator $\hat{o}$ can be calculated from the master equation in Eq. (4) via $\frac{d}{dt}\langle\hat{o}\rangle = {\rm tr}(\hat{o}\dot{\hat{\rho}})$. Combining the commutation relations of operators $[\hat{i}, \hat{j}^\dagger] = \delta_{i,j}$, $[\hat{i}, \hat{j}] = 0$, and $[\hat{i}^\dagger, \hat{j}^\dagger] = 0$ $(\hat{i}, \hat{j} =$

$\hat{a}, \hat{b}$), the equations of motion of $\langle\hat{a}\rangle$ and $\langle\hat{b}\rangle$ can be obtained as

$$\frac{d}{dt}\langle\hat{a}\rangle = -i\Delta\langle\hat{a}\rangle + iG\langle\hat{b}\rangle - \kappa\langle\hat{a}\rangle, \tag{5a}$$

$$\frac{d}{dt}\langle\hat{b}\rangle = -i\omega_m\langle\hat{b}\rangle + iG\langle\hat{a}\rangle + \gamma\langle\hat{b}\rangle. \tag{5b}$$

Correspondingly, the equations of motion of forms $\langle\hat{i}^\dagger\hat{j}\rangle$ are given by

$$\frac{d}{dt}\langle\hat{a}^\dagger\hat{b}\rangle = (i\Delta - i\omega_m - \kappa + \gamma)\langle\hat{a}^\dagger\hat{b}\rangle + iG(\langle\hat{a}^\dagger\hat{a}\rangle - \langle\hat{b}^\dagger\hat{b}\rangle), \tag{6a}$$

$$\frac{d}{dt}\langle\hat{a}^\dagger\hat{a}\rangle = -2\kappa\langle\hat{a}^\dagger\hat{a}\rangle + iG\langle\hat{a}^\dagger\hat{b}\rangle - iG\langle\hat{a}\hat{b}^\dagger\rangle, \tag{6b}$$

$$\frac{d}{dt}\langle\hat{b}^\dagger\hat{b}\rangle = 2\gamma\langle\hat{b}^\dagger\hat{b}\rangle - iG\langle\hat{a}^\dagger\hat{b}\rangle + iG\langle\hat{a}\hat{b}^\dagger\rangle + 2\gamma. \tag{6c}$$

III. $\mathcal{PT}$ SYMMETRY AND STABILITY

A. $\mathcal{PT}$ symmetry

Taking the cavity loss rate κ and the mechanical gain strength γ into consideration, the effective Hamiltonian is obtained as

$$\hat{H}_{\rm eff} = \hbar(\Delta - i\kappa)\hat{a}^\dagger\hat{a} + \hbar(\omega_m + i\gamma)\hat{b}^\dagger\hat{b} - \hbar G(\hat{a}^\dagger\hat{b} + \hat{a}\hat{b}^\dagger). \tag{7}$$

The properties of the space reflection (parity) operator $\mathcal{P}$ and the time-reversal operator $\mathcal{T}$ are demonstrated as follows [46–48]. The action of the parity operator $\mathcal{P}$ on $\hat{H}_{\rm eff}$ is given by [55,58]

$$\mathcal{P}: \hat{a} \leftrightarrow -\hat{b},\ \hat{a}^\dagger \leftrightarrow -\hat{b}^\dagger, \tag{8}$$

and the action of the time-reversal operator $\mathcal{T}$ on $\hat{H}_{\rm eff}$ is

$$\mathcal{T}: \hat{a} \leftrightarrow \hat{a},\ \hat{a}^\dagger \leftrightarrow \hat{a}^\dagger,\ \hat{b} \leftrightarrow \hat{b},\ \hat{b}^\dagger \leftrightarrow \hat{b}^\dagger,\ i \leftrightarrow -i. \tag{9}$$

After the combined actions of the parity and time-reversal operations, i.e., the $\mathcal{PT}$ operations, the effective Hamiltonian in Eq. (7) becomes

$$\begin{aligned}\hat{H}_{\rm eff}^{\mathcal{PT}} &= \mathcal{PT}\hat{H}_{\rm eff}(\mathcal{PT})^{-1} \\ &= \hbar(\Delta + i\kappa)\hat{b}^\dagger\hat{b} + \hbar(\omega_m - i\gamma)\hat{a}^\dagger\hat{a} - \hbar G(\hat{a}^\dagger\hat{b} + \hat{a}\hat{b}^\dagger).\end{aligned} \tag{10}$$

From Eq. (10), we can obtain $H_{\rm eff} = H_{\rm eff}^{\mathcal{PT}}$ if and only if the relations $\Delta = \omega_m = \omega_1$ and $\kappa = \gamma$ are satisfied. In fact, the $\mathcal{PT}$ symmetry can be generalized to the case where the cavity decay rate κ is not exactly equal to the mechanical gain strength γ. Therefore, in the latter case, only the relation $\Delta = \omega_m = \omega_1$ is always satisfied. The Hamiltonian of Eq. (7) is rewritten as

$$\hat{H} = \hbar\begin{pmatrix}\hat{a}^\dagger & \hat{b}^\dagger\end{pmatrix}\begin{pmatrix}\omega_1 - i\kappa & -G \\ -G & \omega_1 + i\gamma\end{pmatrix}\begin{pmatrix}\hat{a} \\ \hat{b}\end{pmatrix}. \tag{11}$$

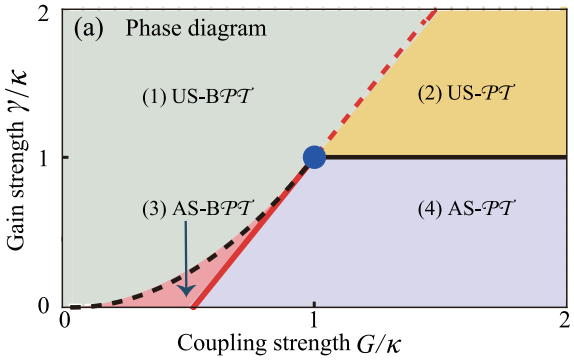

(b)	Broken $\mathcal{PT}$ (B$\mathcal{PT}$) symmetry [$G<(\gamma+\kappa)/2$]	$\mathcal{PT}$-symmetry [$G>(\gamma+\kappa)/2$]	Exceptional -point [$G=(\gamma+\kappa)/2$]
Unstable ($\gamma>\kappa$ or $f<0$)	(1) US-B$\mathcal{PT}$	(2) US-$\mathcal{PT}$	Red dashed line
Asymptotically stable ($\gamma<\kappa$ and $f>0$)	(3) AS-B$\mathcal{PT}$	(4) AS-$\mathcal{PT}$	Red solid line
Stable ($\gamma=\kappa$ or $f=0$)	(5) S-B$\mathcal{PT}$ Black dashed curve	(6) S-$\mathcal{PT}$ Black solid line	**Blue** point

FIG. 2. (a) Phase diagram under different conditions of the mechanical gain rate γ and the effective optomechanical strength $G = g\alpha_s$, in units of the cavity decay rate κ. There are two borders. The red line shows the border between the $\mathcal{PT}$-symmetric phase ($\mathcal{PT}$, on the right hand) and the broken-$\mathcal{PT}$-symmetric phase (B$\mathcal{PT}$, on the left hand). The black dashed curve and black solid line are the border between the asymptotically stable (AS, below the border) phase and the unstable (US, above the border) phase. (b) Various regimes of the $\mathcal{PT}$ symmetry and stability of the system. The new parameter f in the table is defined as $f \equiv G^2 - \gamma\kappa$.

By diagonalizing the matrix in Eq. (11), the eigenfrequencies of the supermodes $\hat{A}_\pm = (\hat{a} \pm \hat{b})$ can be obtained as

$$\omega_\pm = \omega_1 - \frac{i}{2}(\kappa - \gamma) \pm \sqrt{G^2 - \frac{1}{4}(\kappa + \gamma)^2}. \tag{12}$$

When $G > (\kappa + \gamma)/2$, the eigenfrequencies have two different real parts and an identical imaginary part, the system possesses the $\mathcal{PT}$ symmetry with two different frequencies and an identical linewidth, which is described by the regimes (2) and (4) in the phase diagram shown in Fig. 2(a).

If the parameters satisfy the relation $G < (\kappa + \gamma)/2$, the eigenfrequencies have two different imaginary parts and an identical real part. The frequencies of the supermodes are the same, while their linewidths are different. Then the $\mathcal{PT}$ symmetry of the system is broken. The broken-$\mathcal{PT}$ symmetry corresponds to the regimes (1) and (3) in the phase diagram shown in Fig. 2(a).

The phase transition of the $\mathcal{PT}$ symmetry takes place around the border point $G = (\kappa + \gamma)/2$, which is termed as an *exceptional point* (EP) [79–84] as shown by the red line and blue point in the phase diagram. Note that this is a semiclassical EP, which corresponds to a spectral degeneracy of a non-Hermitian Hamiltonian. The prediction of a quantum EP would require the inclusion of quantum noise by finding degeneracies of, e.g., a Liouvillian, as proposed in Refs. [79,81,82].

B. Stability

The linearized equations of motion can be compactly written in a matrix form as

$$\dot{\hat{\mathbf{u}}} = \mathbf{A}\hat{\mathbf{u}}, \tag{13}$$

where $\hat{\mathbf{u}}$ is the column vector of $\hat{\mathbf{u}}^T = (\hat{a}, \hat{a}^\dagger, \hat{b}, \hat{b}^\dagger)$, and the square matrix $\mathbf{A}$ is

$$A = \begin{pmatrix} -i\omega_1 - \kappa & 0 & iG & 0 \\ 0 & i\omega_1 - \kappa & 0 & -iG \\ iG & 0 & -i\omega_1 + \gamma & 0 \\ 0 & -iG & 0 & i\omega_1 + \gamma \end{pmatrix}. \tag{14}$$

The eigenvalues λ of the matrix $\mathbf{A}$ are

$$\lambda_{\tau,s} = \frac{1}{2}[\gamma - \kappa + \tau\sqrt{(\gamma+\kappa)^2 - 4G^2} + is2\omega_1], \tag{15}$$

where $\tau = \pm 1$ and $s = \pm 1$.

The stability of the system can be discussed in the following cases [85,86].

(i) If the parameters satisfy the relations $f < 0$ ($f = G^2 - \gamma\kappa$) or $\gamma > \kappa$, some eigenvalues of A have a positive real part, so the system is unstable. This corresponds to the regimes (1) and (2) in the phase diagram in Fig. 2(a).

(ii) When $f > 0$ and $\gamma < \kappa$, all of the eigenvalues of $\mathbf{A}$ have a negative real part, so the system lies in the asymptotically stable regime. This situation is described by the regimes (3) and (4) in Fig. 2(a).

(iii) When $f = 0$ and $\gamma < \kappa$, the real parts of the two eigenvalues of $\mathbf{A}$ are zero and those of the other two are negative; so the system is stable, and is described by the black dashed curve (5) in Fig. 2(a).

(iv) When $f > 0$ and $\gamma = \kappa$, we find $\lambda_{\tau,s} = \tau\sqrt{\kappa^2 - G^2} + is\omega_1$. In this case, all the eigenvalues of $\mathbf{A}$ have a vanishing real part and the corresponding four eigenvectors are linearly independent; thus, the system is in the finite-time stable regime, but not asymptotically stable, and shown by the black solid curve (6) in Fig. 2(a).

(v) When $f = 0$ and $\gamma = \kappa$, the real parts of the eigenvalues of $\mathbf{A}$ are zero and $\mathbf{A}$ has only two linearly independent eigenvectors. In this case the system is unstable. This corresponds to the blue point in Fig. 2(a).

Note that $\mathcal{PT}$ symmetry and stability of the system can be obtained by analyzing either the eigensystem of the Hamiltonian [given by Eqs. (11) and (12)] or the coefficient matrix $\mathbf{A}$ [given by Eq. (14)] of the linearized Langevin equations. For a non-Hermitian Hamiltonian, its eigenvalues are real or imaginary, which can describe unbroken-$\mathcal{PT}$ symmetry or broken-$\mathcal{PT}$ symmetry. The boundary between the unbroken- and broken-$\mathcal{PT}$ symmetries corresponds to the exceptional point. On the other hand, based on the eigenvalues of the Hamiltonian, the main stability properties can be demonstrated. For example, when the eigenvalue of the Hamiltonian is complex, the system will be exponentially amplified. For the real eigenvalue, the system takes nondecaying oscillations. However, the effects of the noise source and the nonlinearity will be not demonstrated by analyzing the eigenvalues of the Hamiltonian. Thus, we here discuss in detail the stability conditions, based on the coefficient matrix $\mathbf{A}$ of the linearized Langevin equations, via the Routh-Hurwitz criterion [85,86].

IV. DYNAMICS OF THE AVERAGE DISPLACEMENT OF THE MECHANICAL OSCILLATOR

Now, we consider the dynamics of the average displacement of the mechanical oscillator. Here, the initial state of the system is assumed to be a coherent state $|\alpha\rangle|\beta\rangle$, where the amplitudes of the coherent state are given, respectively, by α_0 and β_0 with θ_1 and θ_2 being the initial phases. The average value of the mechanical displacement, $x = \langle\hat{x}\rangle = \sqrt{\hbar/2m\omega_1}(\langle\hat{b}\rangle + \langle\hat{b}\rangle^*)$, can be calculated by solving Eq. (5b) in the case of $\Delta = \omega_m = \omega_1$ as

$$x = \frac{1}{\Omega}\sqrt{\frac{\hbar}{2m\omega_1}}\exp\left[\frac{1}{2}(\gamma - \kappa - 2i\omega_1)t\right]\left[\beta\Omega\cosh\left(\frac{\Omega}{2}t\right) + (\beta\gamma + \beta\kappa + 2iG\alpha)\sinh\left(\frac{\Omega}{2}t\right)\right] + \text{c.c.}, \tag{16}$$

where $\Omega = \sqrt{(\gamma+\kappa)^2 - 4G^2}$, which is an imaginary number in the $\mathcal{PT}$-symmetric regime [$G > (\kappa+\gamma)/2$], and the terms $\cosh(\frac{\Omega}{2}t)$ and $\sinh(\frac{\Omega}{2}t)$ are transformed into the form of a sinusoidal time function; Ω is a real number in the broken-$\mathcal{PT}$-symmetric regime [$G < (\kappa+\gamma)/2$] and the expression can remain the same.

Based on the expression shown in Eq. (16), we investigate the dynamics of the mechanical displacement by plotting the time evolution of the average value of the displacement operator. First, we consider the dynamics of the average displacement in the $\mathcal{PT}$-symmetric regime. In Fig. 3(a), we set the parameters $\gamma = 0.6\kappa$ and $G = 1.2\kappa$ which lead the system to the asymptotically stable regime (4). We can see here that the oscillations of the displacement exhibit collapses and revivals with a decaying amplitude and asymptotically approach zero (at the equilibrium position) for a certain time. When the values of the parameters are set as $\gamma = \kappa$ and $G = 1.5\kappa$, as shown in Fig. 3(b), the system lies in the finite-time stable regime (6), but not asymptotically stable. It is shown here that the oscillations of the average displacement exhibit collapses and revivals periodically. The dynamical behavior of the average displacement in the unstable regime (2) are displayed in Fig. 3(c) with the parameters given by $\gamma = 1.8\kappa$ and $G = 2.1\kappa$. It is shown that the average displacement of the mechanical oscillator oscillates with periodic collapses and revivals with increasing amplitude.

Second, we consider the dynamical evolution of the average displacement in the broken-$\mathcal{PT}$-symmetric regime. In Fig. 3(d), the parameters are set as $\gamma = 0.6\kappa$ and $G = 0.798\kappa$ which enables the system to be in the asymptotically stable regime (3). It is shown that the oscillations of the average displacement increases with time and then decreases to the equilibrium value 0. When the parameters are given by $\gamma = 0.6\kappa$ and $G = \sqrt{0.6}\kappa$, as shown in Fig. 3(e), the system is in the finite-time stable regime (5), the oscillation amplitude of the average displacement increases with time and then approaches the constant value,

$$A_s = \frac{2}{\kappa - \gamma}\sqrt{\frac{\hbar}{2m\omega_1}}[\kappa^2|\beta|^2 + \kappa\gamma|\alpha|^2 - i\kappa\sqrt{\kappa\gamma}(\alpha^*\beta - \beta^*\alpha)]^{\frac{1}{2}}. \tag{17}$$

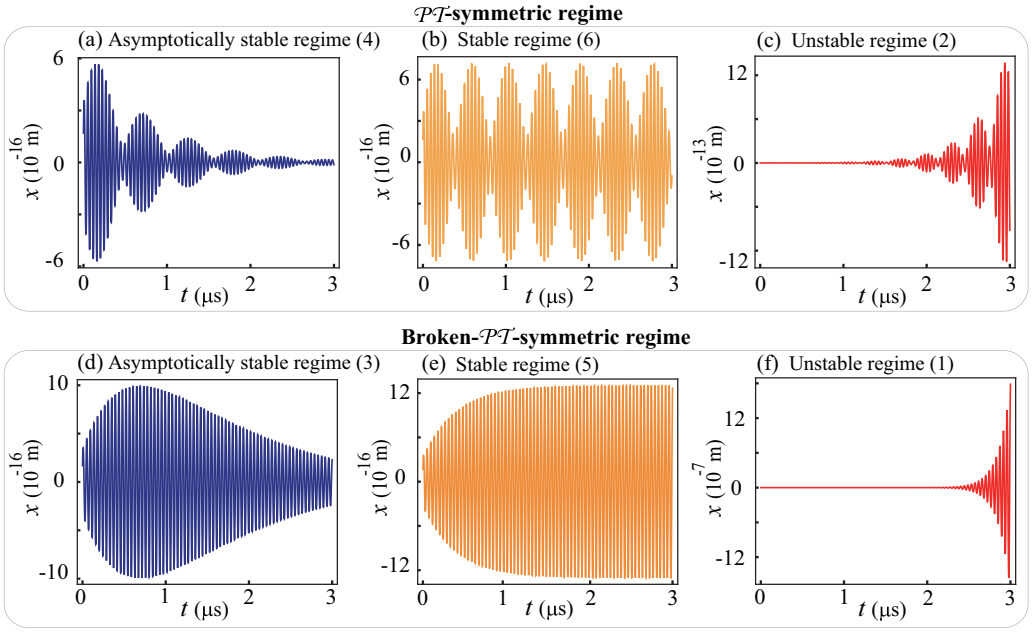

FIG. 3. Dynamics of the average displacement in the $\mathcal{PT}$-symmetric (first row) and broken-$\mathcal{PT}$-symmetric (second row) regimes. Examples for different stable regimes shown in Figs. 2(b) and 2(c): (a) and (d) correspond to the asymptotically stable regime, (b) and (e) correspond to the finite-time stable regime, but not asymptotically stable, (c) and (f) correspond to the unstable regime. The gain rate γ of the mechanical oscillator and the effective optomechanical coupling strength G are given by (a) $\gamma = 0.6\kappa$ and $G = 1.2\kappa$, (b) $\gamma = \kappa$ and $G = 1.5\kappa$, (c) $\gamma = 1.8\kappa$ and $G = 2.1\kappa$, (d) $\gamma = 0.6\kappa$ and $G = 0.798\kappa$, (e) $\gamma = 0.6\kappa$ and $G = \sqrt{0.6}\kappa$, (f) $\gamma = 1.8\kappa$ and $G = 1.2\kappa$. Other parameters are set as $\kappa = 6.45$MHz, $m = 5 \times 10^{-11}$kg, $\omega_1 = 23.4 \times 2\pi$MHz [55,58], $\alpha = 2\exp(i\pi/6)$, and $\beta = 2\exp(i\pi/3)$.

In Fig. 3(f), we consider the dynamical evolution of the average displacement in the unstable regime (1) with parameter $\gamma = 1.8\kappa$ and $G = 1.2\kappa$. In this regime (f), the average displacement oscillates with an increasing amplitude with time.

By comparing the dynamics in the $\mathcal{PT}$-symmetric regime, shown in Figs. 3(a)–3(c), with those in the broken-$\mathcal{PT}$-symmetric regime, shown in Figs. 3(d)–3(f), we can see that the periodic collapses and revivals appear in the former case, while they do not exist in the latter case. In the three stable regimes, the different types of the dynamical behavior exhibit amplitude oscillations with time. Specifically, the oscillation amplitude of the average displacement x decreases to 0 as $t \to \infty$ when the system is asymptotically stable [regimes (3) and (4)]. However, the oscillation amplitude exponentially grows in the unstable regimes (1) and (2). While it periodically oscillates, with a constant amplitude, when the system is finite-time stable, but not asymptotically stable [regimes (5) and (6)]. These results open up an avenue to the manipulation of the mechanical motion by utilizing $\mathcal{PT}$-symmetric optomechanical devices.

V. DYNAMICS OF THE AVERAGE PARTICLE NUMBERS

In the following, we discuss the dynamics of the average particle numbers in terms of the photon number $n_a = \langle \hat{a}^\dagger \hat{a} \rangle$ and the phonon number $n_b = \langle \hat{b}^\dagger \hat{b} \rangle$ by solving Eq. (6c) evolving from a coherent state $|\alpha\rangle|\beta\rangle$ under the condition $\Delta = \omega_m = \omega_1$. In order to understand the source of the generated particles more clearly, we divide the total average particle numbers n_i ($i = a, b$) into two parts:

$$n_i = n_i^{\rm st} + n_i^{\rm sp}, \tag{18}$$

where $n_i^{\rm st}$ is the number of particles generated by stimulated emission, which depends on the initial values, and quantum noises are not considered. This part can be obtained from a semiclassical theory. The other term $n_i^{\rm sp}$ is the number of particles generated by spontaneous emission, which is induced by quantum noise [74,77]. We shall investigate the dynamics in the two cases $\gamma = \kappa$ and $\gamma \neq \kappa$, in which the expressions of the average numbers are different.

A. Dynamics of the average particle numbers for $\gamma = \kappa$

First, we consider the dynamics of the average numbers of particles, n_a and n_b, in the case of $\gamma = \kappa$. The expressions of the photon numbers generated by stimulated emission $n_i^{\rm st}$ and spontaneous emission $n_i^{\rm sp}$ are given by

$$\begin{aligned} n_a^{\rm st} &= \frac{1}{4\Omega_1^2}[m_1 + 2o_1 C_1 + 2o_2 S_1], \\ n_b^{\rm st} &= \frac{1}{4\Omega_1^2}[m_1 + 2o_3 C_1 + 2o_4 S_1], \\ n_a^{\rm sp} &= \frac{1}{4\Omega_1^2}\left[-4G^2\kappa t + 2\frac{\kappa G^2}{\Omega_1} S_1\right], \\ n_b^{\rm sp} &= \frac{1}{4\Omega_1^2}\left[-4G^2\kappa t + 4\kappa^2(C_1 - 1) + 2\left(\kappa\Omega_1 + \frac{\kappa^3}{\Omega_1}\right) S_1\right], \end{aligned} \tag{19}$$

where $C_1 = \cosh(2\Omega_1 t)$ and $S_1 = \sinh(2\Omega_1 t)$, with $\Omega_1 = \sqrt{\kappa^2 - G^2}$; Ω_1 is imaginary in the $\mathcal{PT}$-symmetric regime, and the terms C_1 and S_1 transform into the form of a sinusoidal

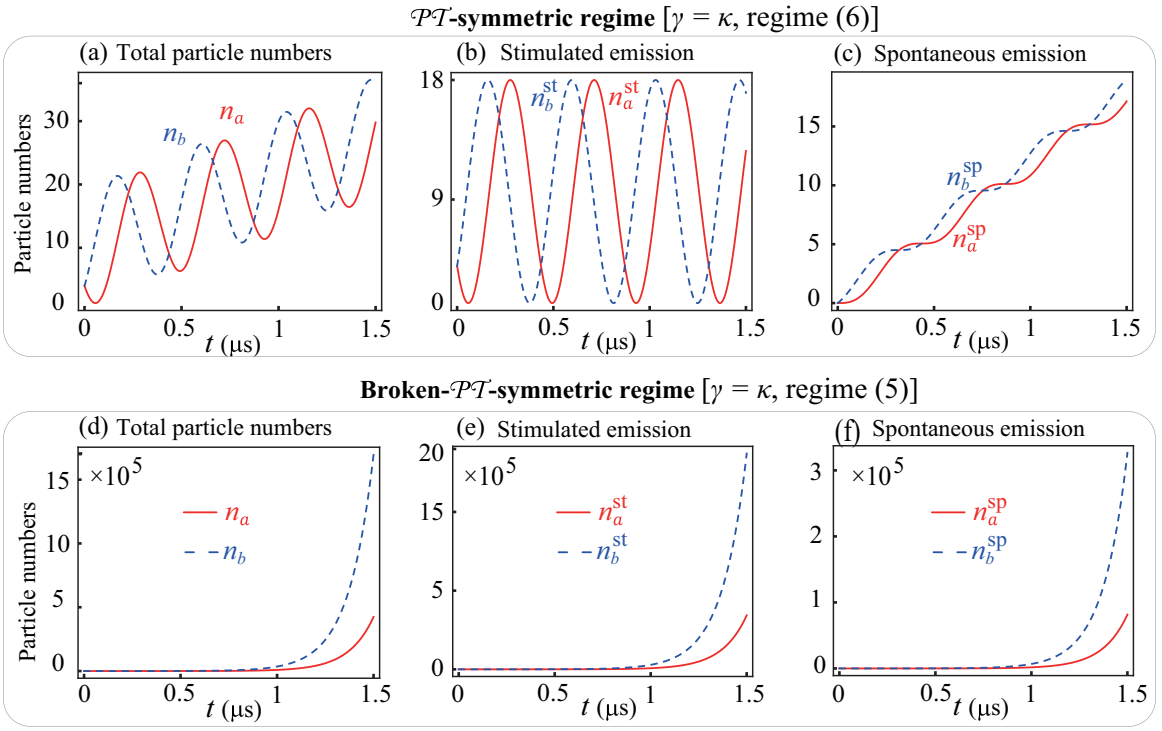

FIG. 4. The dynamics of the photon numbers (solid red curves) and phonon numbers (dashed blue curves) for the $\mathcal{PT}$-symmetric regime (first row with $G = 1.5\kappa$) and the broken-$\mathcal{PT}$-symmetric regime (second row with $G = 0.8$) in the case of $\gamma = \kappa$. The total average particle numbers n_a and n_b are given by (a) and (d); the numbers of particles generated by stimulated generation, $n_a^{\rm st}$ and $n_b^{\rm st}$, are given by (b) and (e); and those generated by spontaneous emission, $n_a^{\rm sp}$ and $n_b^{\rm sp}$, are given by (c) and (f), respectively. Other parameters are the same as Fig. 3.

time function, while Ω_1 is real in the broken-$\mathcal{PT}$-symmetric regime and the expression remains the same. Other coefficients are as follows:

$$\begin{aligned} m_1 &= 2i\kappa\delta - 2G^2(|\alpha|^2 + |\beta|^2), \\ o_1 &= \left(\kappa^2 + \Omega_1^2\right)|\alpha|^2 + G^2|\beta|^2 - i\kappa\delta, \\ o_2 &= i\Omega_1\delta - 2\kappa\Omega_1|\alpha|^2, \\ o_3 &= \left(\kappa^2 + \Omega_1^2\right)|\beta|^2 + G^2|\alpha|^2 - i\kappa\delta, \\ o_4 &= -i\Omega_1\delta + 2\kappa\Omega_1|\beta|^2, \end{aligned} \tag{20}$$

where $\delta = G(\alpha^*\beta - \beta^*\alpha)$.

In the case of $\gamma = \kappa$, the system remains in the two regimes: (i) the finite-time stable regime, but not asymptotically stable and the $\mathcal{PT}$-symmetric regime, when the parameters satisfy the relation of $G > (\kappa + \gamma)/2$ [the regime (6)]; and (ii) the unstable and broken-$\mathcal{PT}$-symmetric regimes for $G < (\kappa + \gamma)/2$ [the regime (5)].

In the regime (6), it is shown in Figs. 4(a)–4(c) that the photon numbers (red solid curve) and phonons (blue dashed curve) oscillate periodically with a monotonously increasing equilibrium value. This is quite different from the dynamics around the constant value in the semiclassical theory (correspond to stimulated generation), and the phenomenon of the monotonically increasing photon and phonon numbers generated by spontaneous generation. The average particle numbers from spontaneous generation dominate the total generation of the average particle numbers after a long-enough time.

From Figs. 4(d)–4(f), it is seen that the average particle numbers increase exponentially with time but without oscillations in the regime (5). Although the average particle numbers from spontaneous generation play an important role in the total number of particles, they do not dominate the total generation of the average particle numbers. We can see from Eq. (19) that the contribution of spontaneous emission decreases as the initial value increases in this case. Our findings indicate that $\mathcal{PT}$-symmetric optomechanical devices can serve as a powerful tool for controlling photons and phonons.

Compared with the previous work [74] focused on the dynamics of photons in $\mathcal{PT}$-symmetric optical systems, our work does not only study the dynamics of both photons and phonons, but also reveals in detail the phase diagram shown in Fig. 2, which has nine different regimes depending on the gain-to-loss ratio and the coupling strength. We show in detail (i) the dynamics of particles (i.e., photons and phonons) generated by both stimulated generation and spontaneous emission; and (ii) the dynamics of the total average particle numbers. Note that spontaneous generation of both photons and phonons is discussed both in the gain-loss balanced (see Fig. 4) and unbalanced (see Figs. 5 and 6) regimes.

B. Dynamics of the average particle numbers for $\gamma \neq \kappa$

Now, we investigate the dynamical behavior of the average particle numbers, n_a and n_b, when $\gamma \neq \kappa$. The expressions of the average particle numbers are given by

$$\begin{aligned} n_a^{\rm st} &= \frac{E_t}{d\Omega^2}(m_2 + 2l_1C + 2l_2S), \\ n_b^{\rm st} &= \frac{E_t}{d\Omega^2}(m_2 + 2l_3C + 2l_4S), \end{aligned}$$

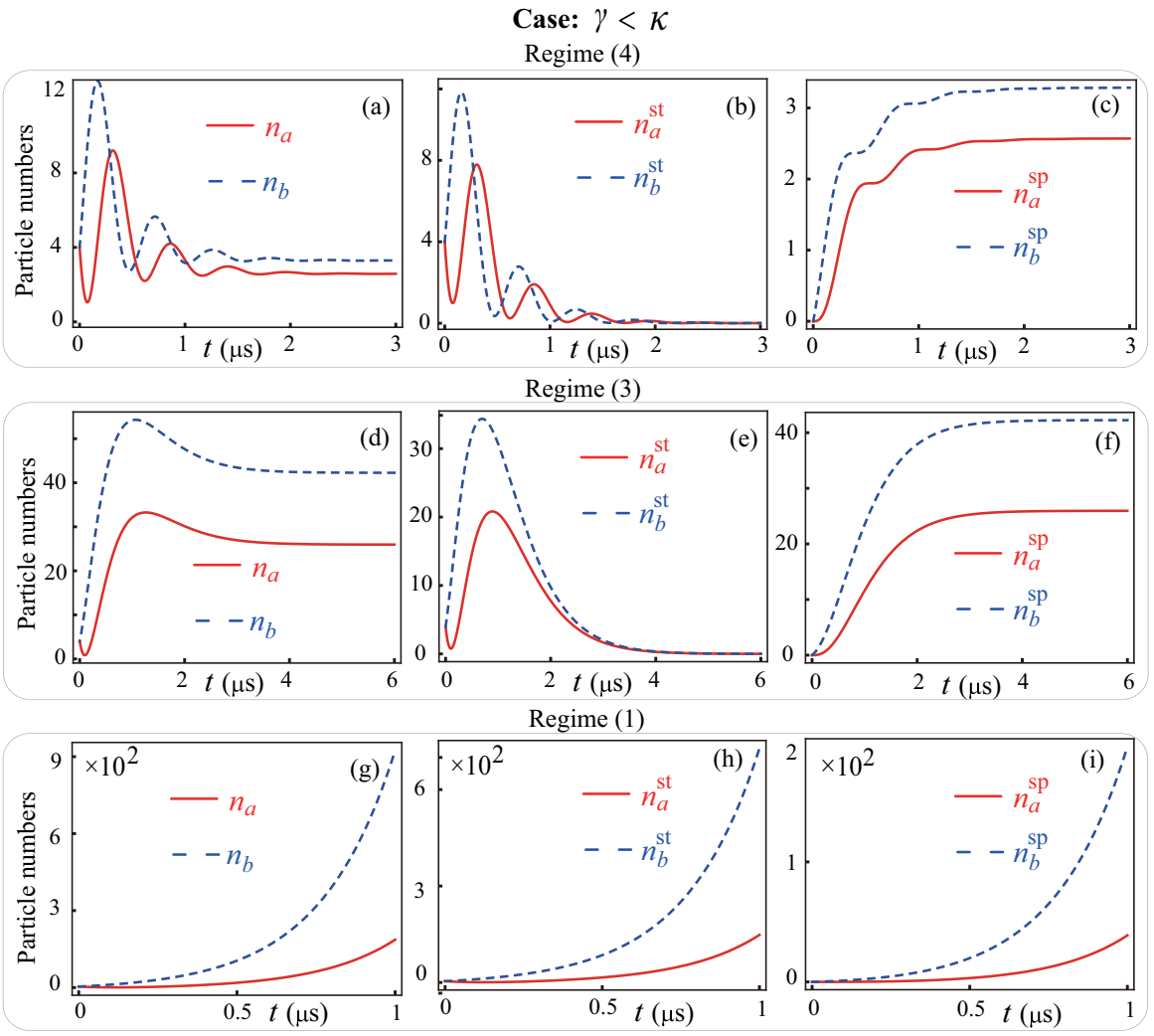

FIG. 5. Dynamics of photons (solid red curves) and phonons (dashed blue curves); (a), (d), (g) show the total average particle numbers n_a and n_b; (b), (e), (h) those generated by stimulated emission, n_a^{st} and n_b^{st}; and (c), (f), (i) these photons and phonons generated by spontaneous emission, n_a^{sp} and n_b^{sp}, when $\gamma < \kappa$. Here we assumed different values of the gain rate γ and the effective optomechanical coupling strength G: (a)–(c) $\gamma = 0.6\kappa$ and $G = 1.2\kappa$, (d)–(f) $\gamma = 0.6\kappa$ and $G = 0.798\kappa$, (g)–(i) $\gamma = 0.6\kappa$ and $G = 0.6\kappa$. Other parameters are the same as Fig. 3.

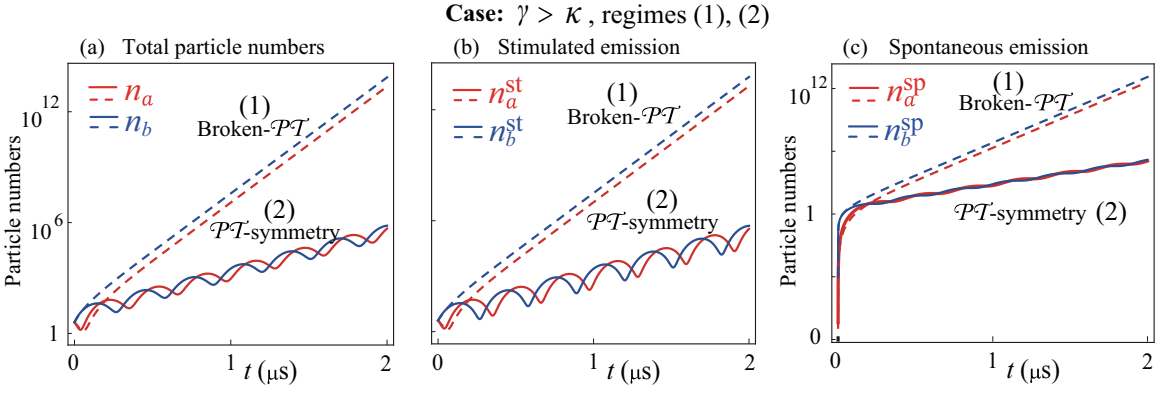

FIG. 6. Dynamics of photons (red curves) and phonons (blue curves) for the $\mathcal{PT}$-symmetric (solid curves) and broken-$\mathcal{PT}$-symmetric (dashed curves) regimes in the case of $\gamma > \kappa$. (a) The total average particle numbers n_a and n_b, (b) the particle numbers generated by stimulated emission, n_a^{st} and n_b^{st}, and (c) those generated by spontaneous emission, n_a^{sp} and n_b^{sp}. Here, the $\mathcal{PT}$-symmetric case is shown for $\gamma = 1.8\kappa$ and $G = 2.1\kappa$, and the broken-$\mathcal{PT}$-symmetric case is shown for $\gamma = 1.8\kappa$ and $G = 1.2\kappa$. Other parameters are the same as in Fig. 3.

$$n_a^{\rm sp} = \frac{4\gamma G^2}{d\Omega^2}E_t[(\gamma-\kappa)^2 C - \Omega(\gamma-\kappa)S - 4f] - \frac{4\gamma G^2}{d},$$
$$n_b^{\rm sp} = \frac{4\gamma(\gamma-\kappa)G^2}{d\Omega^2}E_t\left[\left(\gamma-\kappa-\frac{\kappa\Omega^2}{G^2}\right)C - \frac{4f}{(\gamma-\kappa)} - \frac{\kappa^2-f}{G^2}\Omega S\right] - \frac{4}{d}\gamma(\kappa^2+f), \quad (21)$$

where $E_t = \exp[(\gamma-\kappa)t]$, $C = \cosh(\Omega t)$, and $S = \sinh(\Omega t)$. Similarly to the former case, Ω is imaginary in the $\mathcal{PT}$-symmetric regime, and the terms C and S transform into the form of sinusoidal time function; while Ω is real in the broken-$\mathcal{PT}$-symmetric regime and the expression remains the same. Other coefficients are

$$\begin{aligned} d &= 4(\gamma-\kappa)f, \\ m_2 &= 4f\left[i(\gamma^2-\kappa^2)\delta + 2G^2(\kappa-\gamma)(|\alpha|^2+|\beta|^2)\right], \\ l_1 &= 2(\gamma-\kappa)f\left[(\Omega^2+2G^2)|\alpha|^2 + 2G^2|\beta|^2 - i(\kappa+\gamma)\delta\right], \\ l_2 &= 2\Omega(\gamma-\kappa)f\left[i\delta - (\kappa+\gamma)|\alpha|^2\right], \\ l_3 &= 2(\gamma-\kappa)f\left[2G^2|\alpha|^2 + (\Omega^2+2G^2)|\beta|^2 - i(\kappa+\gamma)\delta\right], \\ l_4 &= 2\Omega(\gamma-\kappa)f[(\kappa+\gamma)|\beta|^2 - i\delta]. \end{aligned} \quad (22)$$

When $\gamma < \kappa$ and $f > 0$, the system lies in the asymptotically stable regime. Meantime, the parameters satisfy the relation $G > (\gamma+\kappa)/2$, the system is $\mathcal{PT}$ symmetric corresponding to the regime (4), which is illustrated by Figs. 5(a)–5(c). These figures show that the total average particle numbers oscillate in different phase regimes in a certain interval after which it asymptotically approaches an equilibrium value. The oscillation behavior is mainly contributed by the average particle numbers of stimulated generation, while the equilibrium values are only determined by spontaneous generation.

On the other hand, if the parameters satisfy the relation $G < (\gamma+\kappa)/2$, the system is in the broken-$\mathcal{PT}$-symmetric regime [the regime (3)], which is illustrated by Figs. 5(d)–5(f). Here, the average particle numbers of stimulated generation start to increase with time, and then decrease to zero; the average particle numbers due to spontaneous generation increase with time and reach an equilibrium value.

When $f < 0$ and $G < (\gamma+\kappa)/2$, the system is in the unstable and broken-$\mathcal{PT}$-symmetric regimes [the regime (1)], which are shown in Figs. 5(g)–5(i). The average particle numbers increase exponentially with time, and the spontaneous generation plays an important role only in the total average particle numbers. From Eq. (21) we find that the contribution from spontaneous emission decreases with the initial values.

When the parameters satisfy the relation $\gamma > \kappa$, the system is always unstable, the average particle numbers n_a and n_b have periodic oscillation and their amplitudes increase exponentially with time in the $\mathcal{PT}$-symmetric regime (2), while the oscillation disappears in the broken-$\mathcal{PT}$-symmetric regime (1), which are shown in Fig. 6, respectively. The effect of spontaneous generation on the average particle numbers also decreases with the initial values when $\gamma > \kappa$.

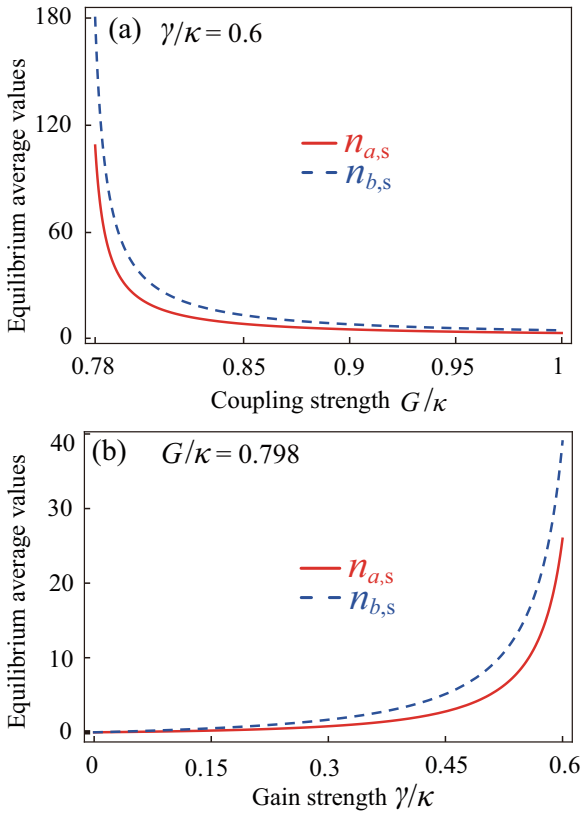

FIG. 7. (a) Equilibrium average values $n_{a,s}$ (solid red curves) and $n_{b,s}$ (dashed blue curves) with respect to the dimensionless normalized coupling strength G/κ when $\gamma = 0.6\kappa$. (b) Equilibrium values of $n_{a,s}$ (solid red curve) and $n_{b,s}$ (dashed blue curve) with respect to the dimensionless normalized gain strength γ/κ when $G = 0.798\kappa$.

We also consider the steady behavior of the average particle numbers n_a and n_b, which are given by

$$n_{a,s} = \frac{G^2\gamma}{(\kappa-\gamma)f}, \quad (23a)$$
$$n_{b,s} = n_{a,s} + \frac{\kappa\gamma}{f}. \quad (23b)$$

From Eqs. (23a) and (23b), the equilibrium values $n_{a,s}$ and $n_{b,s}$ are independent of their initial values. We consider the variations of the steady values with the normalized coupling strength G/κ and normalized gain strength γ/κ, which are shown in Figs. 7(a) and 7(b). It is seen that the steady-state values $n_{a,s}$ and $n_{b,s}$ decrease with G and approach $\gamma/(\kappa-\gamma)$, while the $n_{a,s}$ and $n_{b,s}$ increase with γ/κ.

VI. DISCUSSIONS

Finally, we here discuss a generalization of the present study to a general gain-loss model. Based on the fact that the linearized Hamiltonian in this work is not unique to cavity optomechanics, we can extend the present method to a general model for gain-loss coupled systems, e.g., two oscillators, waveguides, or cavities. This is because the related dynamics of a general coupled two-mode system has flexibility and scalability. Recently, the dynamics in the $\mathcal{PT}$-symmetric regime

TABLE I. Different ways of realizing the mechanical gain. Its value is also listed. The eleven symbols used here are explicitly described in Table II.

Method	Effective mechanical gain $\gamma_{\rm eff}$	Value
Coupled with a blue-detuned phonon cavity [91]	$\frac{4\lvert G_{\rm ph}\rvert^2}{\gamma_m}$	$\sim$10 Hz
Phonon lasing with NV centers [92]	$\frac{4\lambda_\perp^2\Gamma\Omega^2}{(\Gamma^2+4\lambda_\perp^2 r)^2}$	$\sim 10^3$ Hz
Adiabatically eliminating a blue-detuned cavity [77]	$\frac{4G^2}{\kappa}\frac{16\omega_{\rm m}^2}{\kappa^2+16\omega_{\rm m}^2}+\gamma_{\rm m}$	$\sim 10^5$ Hz
Photoelastic scattered by two-optical modes [51,93]	$\frac{G^2}{\kappa_{\rm a}}$	$\sim 10^6$ Hz

has been studied in coupled cavities [55,75,76,87], two coupled fiber loops [88], two coupled waveguides [74,89,90], in which the discussed mechanism can also be observed.

Moreover, we have added two tables to show several means of realizing the mechanical gain with different value scales, as shown in Tables I and II. It shows that the $\mathcal{PT}$-symmetry optomechanics has a flexible gain, which can be generalized to an arbitrary coupled two-oscillator/waveguide system.

Let us also briefly discuss an experimental realization of our system. In the optical domain, a generic optomechanical system consists of a laser-driven optical cavity and a vibrating-end mirror [1–3]. In the microwave domain, it consists of a vibrating capacitor, where a microwave drive is applied along a transmission line that is inductively coupled to the *LC* circuit representing a microwave resonator [1–3]. At present, typical cavity optomechanical systems have been experimentally implemented by employing cantilevers, micromirrors, microcavities, nanomembranes, and macroscopic mirror modes [1,2]. For example, in the membrane-in-the-middle setup, a mechanical membrane is inserted between two fixed cavity mirrors, and this mechanical membrane can be coupled to the cavity mode via radiation-pressure interaction [2]. In the Fabry-Pérot cavity optomechanical configurations, composed of a movable mirror and a fixed mirror, the movable mirror is coupled to a single optical mode through an optomechanical coupling [2]. Currently, the active mechanical resonator can be implemented by a mechanical gain, which can be realized by using phonon lasing, a blue-detuned optical pump, or a direct driving of the mechanical mode [51,78]. In addition, two tables are presented to show in detail various methods for realizing the mechanical gain, as shown in Tables I and II.

TABLE II. The eleven symbols used in Table I.

Symbol	Parameter
κ	Decay rate of the optical cavity
$\gamma_{\rm m}$	Mechanical damping rate
$\gamma_{\rm eff}$	Effective mechanical gain
$\kappa_{\rm a}$	Average decay rate of the optical modes
$G_{\rm ph}$	Parametric intermodal coupling
G	Effective optomechanical coupling
Γ	Radiative decay of the NV defect
Ω	Rabi frequency
$\lambda_\perp$	Coupling between the vibrational modes
$\omega_{\rm m}$	Mechanical frequency
r	Amplitude of the coherent state

VII. CONCLUSIONS

In summary, we have theoretically investigated the dynamics of the average numbers of particles (i.e., photons and phonons) and the average value of the displacement of the mechanical resonator for a $\mathcal{PT}$-symmetric-like optomechanical system. The analytical expressions of these quantities were obtained from the master equation in the full quantum regime, including quantum noise. The dynamics of the number of particles and displacement in different regimes have shown the following characteristics of each regime.

(i) In the $\mathcal{PT}$-symmetric regime, the energy is exchanged rapidly between the cavity and the mechanical oscillator. Moreover, the periodic collapse and revival of the average displacement and the oscillations of the average particle numbers were obtained. In contrast to this regime, all of the studied averages disappear in the broken-$\mathcal{PT}$-symmetric regime.

(ii) In the asymptotically stable regime, the average displacement and the average particle numbers reach their equilibrium values after some evolution time. The average displacement oscillates periodically around zero, and the average particle numbers also oscillate with a monotonously increasing equilibrium value in the finite-time stable regimes (5) and (6), but not asymptotically stable. In the unstable regime, both average particle numbers and displacement increase exponentially.

(iii) Spontaneous emission does not only play an important role for the case of $\gamma=\kappa$, but also for the case of $\gamma\neq\kappa$. And this emission dominates the total generation of the average particle numbers after a long enough time in the finite-time stable regime even in the asymptotic limit, while not in the unstable regime. Otherwise, the contribution of spontaneous emission decreases with the initial values.

These results indicate that $\mathcal{PT}$-assisted optomechanical devices can provide a versatile platform to manipulate the mechanical motion, photons, and phonons.

ACKNOWLEDGMENTS

We thank Prof. Hui Jing for his very useful comments. B.P.H. is supported in part by National Natural Science Foundation of China (Grant No. 11974009). A.M. is supported by the Polish National Science Centre (NCN) under the Maestro Grant No. DEC-2019/34/A/ST2/00081. F.N. is supported in part by Nippon Telegraph and Telephone Corporation (NTT) Research, the Japan Science and Technology Agency (JST) [via the Quantum Leap Flagship Program (Q-LEAP) program, the Moonshot R&D Grant No. JPMJMS2061, and the Centers of Research Excellence in Science and Technology (CREST)

Grant No. JPMJCR1676], the Japan Society for the Promotion of Science (JSPS) [via the Grants-in-Aid for Scientific Research (KAKENHI) Grant No. JP20H00134 and the JSPS CRFBR Grant No. JPJSBP120194828], the Army Research Office (ARO) (Grant No. W911NF-18-1-0358), the Asian Office of Aerospace Research and Development (AOARD) (via Grant No. FA2386-20-1-4069), and the Foundational Questions Institute Fund (FQXi) via Grant No. FQXi-IAF19-06.

APPENDIX A: DERIVATION FROM EQ. (1) TO EQ. (2)

In this Appendix, we show in detail how to obtain Eq. (2) from Eq. (1). Based on Eq. (1), the equations of motion of the system, which include the gain and loss terms, are

$$\frac{d\hat{a}}{dt} = -i\Delta_c\hat{a} + ig\hat{a}(\hat{b}+\hat{b}^\dagger) + \Omega_L - \kappa\hat{a}, \tag{A1}$$

$$\frac{d\hat{b}}{dt} = -i\omega_m\hat{b} + ig\hat{a}^\dagger\hat{a} + \gamma\hat{b}. \tag{A2}$$

Here, we consider the strong-driving regime for the cavity, so that our physical model can be simplified by a linearization procedure. Then, we write the operators in Eqs. (A1) and (A2) as the sums of the steady-state averages and the quantum fluctuations: $\hat{a} = \alpha_s + \delta\hat{a}$ and $\hat{b} = \beta_s + \delta\hat{b}$. By separating the quantum fluctuations and the classical motion, we can obtain the classical equations of motion:

$$\frac{d\alpha_s}{dt} = -i\Delta_c\alpha_s + ig\alpha_s(\beta_s+\beta_s^*) + \Omega_L - \kappa\alpha_s, \tag{A3}$$

$$\frac{d\beta_s}{dt} = -i\omega_m\beta_s + ig\alpha_s^*\alpha_s + \gamma\beta_s. \tag{A4}$$

By setting the left-hand sides of Eqs. (A3) and (A4) equal to zero, the steady-state mean values of the dynamical variables can be obtained as

$$\alpha_s = \frac{\Omega_L}{i\Delta+\kappa}, \quad \beta_s = \frac{ig\alpha_s^*\alpha_s}{i\omega_m-\gamma}, \tag{A5}$$

where $\Delta = \Delta_c - g(\beta_s+\beta_s^*)$ is the normalized detuning of the cavity field.

Then, the equations of motion for quantum fluctuations can be obtained as

$$\frac{d}{dt}\delta\hat{a} = -i\Delta_c\delta\hat{a} + ig\delta\hat{a}(\beta_s+\beta_s^*) + iga_s(\delta\hat{b}+\delta\hat{b}^\dagger) - \kappa\delta\hat{a}, \tag{A6}$$

$$\frac{d}{dt}\delta\hat{b} = -i\omega_m\delta\hat{b} + iga_s^*\delta\hat{a} + iga_s\delta\hat{a}^\dagger + \gamma\delta\hat{b}, \tag{A7}$$

where the strong driving field has been considered. Thus, the higher order terms of the fluctuation parts could have been neglected safely. Then, using the Langevin equations,

$$\frac{d}{dt}\delta\hat{a} = \frac{1}{i\hbar}[\delta\hat{a}, \hat{H}_{\rm f}] - \kappa\delta\hat{a}, \tag{A8}$$

$$\frac{d}{dt}\delta\hat{b} = \frac{1}{i\hbar}[\delta\hat{b}, \hat{H}_{\rm f}] + \gamma\delta\hat{b}, \tag{A9}$$

and applying the rotating wave approximation (RWA), we can obtain the Hamitonian of the quantum fluctuation parts as

$$\hat{H}_{\rm f} = \hbar\Delta\delta\hat{a}^\dagger\delta\hat{a} + \hbar\omega_m\delta\hat{b}^\dagger\delta\hat{b} - \hbar G(\delta\hat{a}^\dagger\delta\hat{b} + \delta\hat{a}\delta\hat{b}^\dagger), \tag{A10}$$

where $G = g\alpha_s$ is the effective optomechanical coupling strength. The symbol "δ" is always dropped, because we are concerned about the fluctuation parts of system. Then, the so-called "linearized" optomechanical Hamiltonian is obtained from Eq. (A10) as

$$\hat{H}_{\rm lin} = \hbar\Delta\hat{a}^\dagger\hat{a} + \hbar\omega_m\hat{b}^\dagger\hat{b} - \hbar G(\hat{a}^\dagger\hat{b} + \hat{a}\hat{b}^\dagger). \tag{A11}$$

APPENDIX B: MORE DETAILS OF EQ. (7)

Here, we present more details on the derivation of Eq. (7). When the system includes the loss of cavity field and the mechanical gain, the Langevin equations of the quantum fluctuation parts of the total system are

$$\frac{d}{dt}\delta\hat{a} = \frac{1}{i\hbar}[\delta\hat{a}, \delta\hat{H}_{\rm eff}], \tag{B1}$$

$$\frac{d}{dt}\delta\hat{b} = \frac{1}{i\hbar}[\delta\hat{b}, \delta\hat{H}_{\rm eff}]. \tag{B2}$$

By combining Eqs. (A6) and (A7), and Eqs. (B1) and (B2), and applying the RWA, the effective Hamiltonian of the total system is obtained as

$$\hat{H}_{\rm eff} = \hbar(\Delta - i\kappa)\hat{a}^\dagger\hat{a} + \hbar(\omega_m + i\gamma)\hat{b}^\dagger\hat{b} - \hbar G(\hat{a}^\dagger\hat{b} + \hat{a}\hat{b}^\dagger), \tag{B3}$$

where we have dropped the symbol "δ".

[1] T. J. Kippenberg and K. J. Vahala, Cavity optomechanics: Back-action at the mesoscale, Science **321**, 1172 (2008).

[2] M. Aspelmeyer, T. J. Kippenberg, and F. Marquardt, Cavity optomechanics, Rev. Mod. Phys. **86**, 1391 (2014).

[3] T. J. Kippenberg, H. Rokhsari, T. Carmon, A. Scherer, and K. J. Vahala, Analysis of Radiation-Pressure Induced Mechanical Oscillation of an Optical Microcavity, Phys. Rev. Lett. **95**, 033901 (2005).

[4] I. Wilson-Rae, N. Nooshi, W. Zwerger, and T. J. Kippenberg, Theory of Ground State Cooling of a Mechanical Oscillator Using Dynamical Backaction, Phys. Rev. Lett. **99**, 093901 (2007).

[5] F. Marquardt, J. P. Chen, A. A. Clerk, and S. M. Girvin, Quantum Theory of Cavity-Assisted Sideband Cooling of Mechanical Motion, Phys. Rev. Lett. **99**, 093902 (2007).

[6] F. Xue, Y. D. Wang, Y. X. Liu, and F. Nori, Cooling a micromechanical beam by coupling it to a transmission line, Phys. Rev. B **76**, 205302 (2007).

[7] J. Q. You, Y. X. Liu, and F. Nori, Simultaneous Cooling of an Artificial Atom and Its Neighboring Quantum System, Phys. Rev. Lett. **100**, 047001 (2008).

[8] M. Grajcar, S. Ashhab, J. R. Johansson, and F. Nori, Lower limit on the achievable temperature in resonator-based sideband cooling, Phys. Rev. B **78**, 035406 (2008).

[9] M. Bhattacharya and P. Meystre, Trapping and Cooling a Mirror to Its Quantum Mechanical Ground State, Phys. Rev. Lett. **99**, 073601 (2007).

[10] C. Genes, D. Vitali, P. Tombesi, S. Gigan, and M. Aspelmeyer, Ground-state cooling of a micromechanical oscillator: Comparing cold damping and cavity-assisted cooling schemes, Phys. Rev. A **77**, 033804 (2008).

[11] D.-G. Lai, F. Zou, B. P. Hou, Y. F. Xiao, and J. Q. Liao, Simultaneous cooling of coupled mechanical resonators in cavity optomechanics, Phys. Rev. A **98**, 023860 (2018).

[12] C. Sommer and C. Genes, Partial Optomechanical Refrigeration Via Multimode Cold-Damping Feedback, Phys. Rev. Lett. **123**, 203605 (2019).

[13] D.-G. Lai, J. F. Huang, X. L. Yin, B. P. Hou, W. Li, D. Vitali, F. Nori, and J. Q. Liao, Nonreciprocal ground-state cooling of multiple mechanical resonators, Phys. Rev. A **102**, 011502(R) (2020).

[14] C. Sommer, A. Ghosh, and C. Genes, Multimode cold-damping optomechanics with delayed feedback, Phys. Rev. Research **2**, 033299 (2020).

[15] D.-G. Lai, J. Huang, B.-P. Hou, F. Nori, and J.-Q. Liao, Domino cooling of a coupled mechanical-resonator chain via cold-damping feedback, Phys. Rev. A **103**, 063509 (2021).

[16] D.-G. Lai, W. Qin, B.-P. Hou, A. Miranowicz, and F. Nori, Significant enhancement in refrigeration and entanglement in auxiliary-cavity-assisted optomechanical systems, Phys. Rev. A **104**, 043521 (2021).

[17] P. Rabl, Photon Blockade Effect in Optomechanical Systems, Phys. Rev. Lett. **107**, 063601 (2011).

[18] A. Nunnenkamp, K. Børkje, and S. M. Girvin, Single-Photon Optomechanics, Phys. Rev. Lett. **107**, 063602 (2011).

[19] J.-Q. Liao, H. K. Cheung, and C. K. Law, Spectrum of single-photon emission and scattering in cavity optomechanics, Phys. Rev. A **85**, 025803 (2012).

[20] J.-Q. Liao and F. Nori, Photon blockade in quadratically coupled optomechanical systems, Phys. Rev. A **88**, 023853 (2013).

[21] H. Wang, X. Gu, Y.-x. Liu, A. Miranowicz, and F. Nori, Tunable photon blockade in a hybrid system consisting of an optomechanical device coupled to a two-level system, Phys. Rev. A **92**, 033806 (2015).

[22] R. Huang, A. Miranowicz, J.-Q. Liao, F. Nori, and H. Jing, Nonreciprocal Photon Blockade, Phys. Rev. Lett. **121**, 153601 (2018).

[23] B. Li, R. Huang, X. Xu, A. Miranowicz, and H. Jing, Nonreciprocal unconventional photon blockade in a spinning optomechanical system, Photonics Res. **7**, 630 (2019).

[24] F. Zou, L.-B. Fan, J.-F. Huang, and J.-Q. Liao, Enhancement of few-photon optomechanical effects with cross-Kerr nonlinearity, Phys. Rev. A **99**, 043837 (2019).

[25] J.-Q. Liao, J.-F. Huang, L. Tian, L.-Ma. Kuang, and C.-P. Sun, Generalized ultrastrong optomechanical-like coupling, Phys. Rev. A **101**, 063802 (2020).

[26] A. H. Safavi-Naeini, S. Grblacher, J. T. Hill, J. Chan, M. Aspelmeyer, and O. Painter, Squeezed light from a silicon micromechanical resonator, Nature (London) **500**, 185 (2013).

[27] T. P. Purdy, P. L. Yu, R. W. Peterson, N. S. Kampel, and C. A. Regal, Strong Optomechanical Squeezing of Light, Physical Review X **3**, 031012 (2013).

[28] X.-Y. Lü, Y. Wu, J. R. Johansson, H. Jing, J. Zhang, and F. Nori, Squeezed Optomechanics with Phase-Matched Amplification and Dissipation, Phys. Rev. Lett. **114**, 093602 (2015).

[29] L. Liu, B. P. Hou, X. H. Zhao, and B. Tang, Squeezing transfer of light in a two-mode optomechanical system, Opt. Express **27**, 008361 (2018).

[30] W. Qin, A. Miranowicz, P. B. Li, X. Y. Lü, J. Q. You, and F. Nori, Exponentially Enhanced Light-Matter Interaction, Cooperativities, and steady-state Entanglement Using Parametric Amplification, Phys. Rev. Lett. **120**, 093601 (2018).

[31] M. D. LaHaye, O. Buu, B. Camarota, and K. C. Schwab, Approaching the quantum limit of a nanomechanical resonator, Science **304**, 74 (2004).

[32] A. A. Geraci, S. B. Papp, and J. Kitching, Short-Range Force Detection Using Optically Cooled Levitated Microspheres, Phys. Rev. Lett. **105**, 101101 (2010).

[33] A. K. Tagantsev and S. A. Fedorov, Quantum-Limited Measurements Using an Optical Cavity with Modulated Intrinsic Loss, Phys. Rev. Lett. **123**, 043602 (2019).

[34] W. Fu, F. J. Shu, Y. L. Zhang, C. H. Dong, C. L. Zou, and G. C. Guo, Integrated optical circulator by stimulated Brillouin scattering induced non-reciprocal phase shift, Opt. Express **23**, 25118 (2015).

[35] S. Manipatruni, J. T. Robinson, and M. Lipson, Optical Nonreciprocity in Optomechanical Structures, Phys. Rev. Lett. **102**, 213903 (2009).

[36] H. Mohammad and R. Peter, Optomechanically induced nonreciprocity in microring resonators, Opt. Express **20**, 7672 (2012).

[37] X. W. Xu and Y. Li, Optical nonreciprocity and optomechanical circulator in three-mode optomechanical systems, Phys. Rev. A **91**, 053854 (2015).

[38] G. S. Agarwal and S. Huang, Electromagnetically induced transparency in mechanical effects of light, Phys. Rev. A **81**, 041803(R) (2010).

[39] S. Weis, R. Rivière, S. Deléglise, E. Gavartin, O. Arcizet, A. Schliesser, and T. J. Kippenberg, Optomechanically induced transparency, Science **330**, 1520 (2010).

[40] A. H. Safavi-Naeini, T. P. M. Alegre, J. Chan, M. Eichenfield, M. Winger, Q. Lin, J. T. Hill, D. E. Chang, and O. Painter, Electromagnetically induced transparency and slow light with optomechanics, Nature (London) **472**, 69 (2011).

[41] B. P. Hou, L. F. Wei, and S. J. Wang, Optomechanically induced transparency and absorption in hybridized optomechanical systems, Phys. Rev. A **92**, 033829 (2015).

[42] D.-G. Lai, X. Wang, W. Qin, B.-P. Hou, F. Nori, and J.-Q. Liao, Tunable optomechanically induced transparency by controlling the dark-mode effect, Phys. Rev. A **102**, 023707 (2020).

[43] F. Massel, S. U. Cho, J. M. Pirkkalainen, P. J. Hakonen, T. T. Heikkilä, and M. A. Sillanpää, Multimode circuit optomechanics near the quantum limit, Nat. Commun. **3**, 987 (2012).

[44] X. Zhou, F. Hocke, A. Schliesser, A. Marx, H. Huebl, R. Gross, and T. J. Kippenberg, Slowing, advancing and switching of microwave signals using circuit nanoelectromechanics, Nat. Phys. **9**, 179 (2013).

[45] F. Massel, T. T. Heikkilä, J. M. Pirkkalainen, S. U. Cho, H. Saloniemi, P. J. Hakonen, and M. A. Sillanpää, Microwave amplification with nanomechanical resonators, Nature (London) **480**, 351 (2011).

[46] C. M. Bender and S. Boettcher, Real Spectra in Non-Hermitian Hamiltonians Having $\mathcal{PT}$ Symmetry, Phys. Rev. Lett. **80**, 5243 (1998).

[47] C. M. Bender, D. C. Brody, and H. F. Jones, Must a Hamiltonian be Hermitian?, Am. J. Phys. **71**, 1095 (2003).

[48] C. M. Bender, Making sense of non-Hermitian Hamiltonians, Rep. Prog. Phys. **70**, 947 (2007).

[49] C. Y. Ju, A. Miranowicz, G. Y. Chen, and F. Nori, Non-Hermitian Hamiltonians and no-go theorems in quantum information, Phys. Rev. A **100**, 062118 (2019).

[50] C. M. Bender, B. K. Berntson, D. Parker, and E. Samuel, Observation of $\mathcal{PT}$ phase transition in a simple mechanical system, Am. J. Phys. **81**, 173 (2013).

[51] Y. L. Liu, R. B. Wu, J. Zhang, Ş. K. Özdemir, L. Yang, F. Nori, and Y. X. Liu, Controllable optical response by modifying the gain and loss of a mechanical resonator and cavity mode in an optomechanical system, Phys. Rev. A **95**, 013843 (2017).

[52] S. Klaiman, U. Günther, and N. Moiseyev, Visualization of Branch Points in $\mathcal{PT}$-Symmetric Waveguides, Phys. Rev. Lett. **101**, 080402 (2008).

[53] A. Guo, G. J. Salamo, D. Duchesne, R. Morandotti, M. Volatier-Ravat, V. Aimez, G. A. Siviloglou, and D. N. Christodoulides, Observation of $\mathcal{PT}$-Symmetry Breaking in Complex Optical Potentials, Phys. Rev. Lett. **103**, 093902 (2009).

[54] J. Schindler, A. Li, M. C. Zheng, F. M. Ellis, and T. Kottos, Experimental study of active LRC circuits with $\mathcal{PT}$ symmetries, Phys. Rev. A **84**, 040101(R) (2011).

[55] B. Peng, Ş. K. Özdemir, F. Lei, F. Monifi, M. Gianfreda, G. L. Long, S. Fan, F. Nori, C. M. Bender, and L. Yang, Parity-time-symmetric whispering-gallery microcavities, Nat. Phys. **10**, 394 (2014).

[56] H. Jing, Ş. K. Özdemir, X. Y. Lü, J. Zhang, L. Yang, and F. Nori, $\mathcal{PT}$-Symmetric Phonon Laser, Phys. Rev. Lett. **113**, 053604 (2014).

[57] X. Y. Lü, H. Jing, J. Y. Ma, and Y. Wu, $\mathcal{PT}$-Symmetry-Breaking Chaos in Optomechanics, Phys. Rev. Lett. **114**, 253601 (2015).

[58] Ş. K. Özdemir, S. Rotter, F. Nori, and L. Yang, Parity-time symmetry and exceptional points in photonics, Nat. Mater. **18**, 783 (2019).

[59] J. Zhang, B. Peng, Ş. K. Özdemir, Y. X. Liu, H. Jing, X. Y. Lü, Y. L. Liu, L. Yang, and F. Nori, Giant nonlinearity via breaking parity-time symmetry: A route to low-threshold phonon diodes, Phys. Rev. B **92**, 115407 (2015).

[60] Z. P. Liu, J. Zhang, Ş. K. Özdemir, B. Peng, H. Jing, X. Y. Lü, C. W. Li, L. Yang, F. Nori, and Y. X. Liu, Metrology with $\mathcal{PT}$-Symmetric Cavities: Enhanced Sensitivity near the $\mathcal{PT}$-Phase Transition, Phys. Rev. Lett. **117**, 110802 (2016).

[61] F. Quijandría, U. Naether, Ş. K. Özdemir, F. Nori, and D. Zueco, $\mathcal{PT}$-symmetric circuit QED, Phys. Rev. A **97**, 053846 (2018).

[62] I. I. Arkhipov, A. Miranowicz, O. Di Stefano, R. Stassi, S. Savasta, F. Nori, and Ş. K. Özdemir, Scully-Lamb quantum laser model for parity-time-symmetric whispering-gallery microcavities: Gain saturation effects and nonreciprocity, Phys. Rev. A **99**, 053806 (2019).

[63] D. Huybrechts, F. Minganti, F. Nori, M. Wouters, and N. Shammah, Validity of mean-field theory in a dissipative critical system: Liouvillian gap, $\mathcal{PT}$-symmetric antigap, and permutational symmetry in the XYZ model, Phys. Rev. B **101**, 214302 (2020).

[64] H. Zhang, R. Huang, S. D. Zhang, Y. Li, C. W. Qiu, and F. Nori, H. Jing, Breaking anti-$\mathcal{PT}$ symmetry by spinning a resonator, Nano Lett. **20**, 7594 (2020).

[65] H. Lü, Ş. K. Özdemir, L. M. Kuang, F. Nori, and H. Jing, Exceptional Points in Random-Defect Phonon Lasers, Phys. Rev. Appl. **8**, 044020 (2017).

[66] J. Zhang, B. Peng, Ş. K. Özdemir, K. Pichler, D. O. Krimer, G. Zhao, F. Nori, Y. X. Liu, S. Rotter, and L. Yang, A phonon laser operating at an exceptional point, Nat. Photon. **12**, 479 (2018).

[67] H. Jing, Ş. K. Özdemir, Z. Geng, J. Zhang, X. Y. Lü, B. Peng, L. Yang, and F. Nori, Optomechanically-induced transparency in parity-time-symmetric microresonators, Sci. Rep. **5**, 9663 (2015).

[68] H. Jing, Ş. K. Özdemir, H. Lü, and F. Nori, High-order exceptional points in optomechanics, Sci. Rep. **7**, 3386 (2017).

[69] W. Li, Y. Jiang, C. Li, and H. Song, Parity-time-symmetry enhanced optomechanically-induced-transparency, Sci. Rep. **6**, 31095 (2016).

[70] L. Y. He, Parity-time-symmetry-enhanced sideband generation in an optomechanical system, Phys. Rev. A **99**, 033843 (2019).

[71] X. Y. Zhang, Y. Q. Guo, P. Pei, and X. X. Yi, Optomechanically induced absorption in parity-time-symmetric optomechanical systems, Phys. Rev. A **95**, 063825 (2017).

[72] L. Feng, M. Ayache, J. Huang, Y. L. Xu, M. H. Lu, Y. F. Chen, Y. Fainman, and A. Scherer, Nonreciprocal light propagation in a silicon photonic circuit, Science **333**, 729 (2011).

[73] Q. Zhong, S. Nelson, Ş. K. Özdemir, and R. El-Ganainy, Controlling directional absorption with chiral exceptional surfaces, Opt. Lett. **44**, 5242 (2019).

[74] G. S. Agarwal and K. Qu, Spontaneous generation of photons in transmission of quantum fields in $\mathcal{PT}$–symmetric optical systems, Phys. Rev. A **85**, 031802(R) (2012).

[75] D. W. Schönleber, A. Eisfeld, and R. El-Ganainy, Optomechanical interactions in non-Hermitian photonic molecules, New J. Phys. **18**, 045014 (2016).

[76] J. Naikoo, K. Thapliyal, S. Banerjee, and A. Pathak, Quantum Zeno effect and nonclassicality in a $\mathcal{PT}$-symmetric system of coupled cavities, Phys. Rev. A **99**, 023820 (2019).

[77] X. W. Xu, Y. X. Liu, C. P. Sun, and Y. Li, Mechanical $\mathcal{PT}$ symmetry in coupled optomechanical systems, Phys. Rev. A **92**, 013852 (2015).

[78] X. Z. Zhang, L. Tian, and Y. Li, Optomechanical transistor with mechanical gain, Phys. Rev. A **97**, 043818 (2018).

[79] F. Minganti, A. Miranowicz, R. W. Chhajlany, and F. Nori, Quantum exceptional points of non-Hermitian Hamiltonians and Liouvillians: The effects of quantum jumps, Phys. Rev. A **100**, 062131 (2019).

[80] P. C. Kuo, N. Lambert, A. Miranowicz, H. B. Chen, G. Y. Chen, Y. N. Chen, and F. Nori, Collectively induced exceptional points of quantum emitters coupled to nanoparticle surface plasmons, Phys. Rev. A **101**, 013814 (2020).

[81] F. Minganti, A. Miranowicz, R. W. Chhajlany, I. I. Arkhipov, and F. Nori, Hybrid-Liouvillian formalism connecting exceptional points of non-Hermitian Hamiltonians and Liouvillians via postselection of quantum trajectories, Phys. Rev. A **101**, 062112 (2020).

[82] I. I. Arkhipov, A. Miranowicz, F. Minganti, and F. Nori, Liouvillian exceptional points of any order in dissipative linear bosonic systems: Coherence functions and switching between $\mathcal{PT}$ and anti-$\mathcal{PT}$ symmetries, Phys. Rev. A **102**, 033715 (2020).

[83] I. I. Arkhipov, A. Miranowicz, F. Minganti, and F. Nori, Quantum and semiclassical exceptional points of a linear system of coupled cavities with losses and gain within the Scully-Lamb laser theory, Phys. Rev. A **101**, 013812 (2020).

[84] T.-X. Lu, H. Zhang, Q. Zhang, and H. Jing, Exceptional-point-engineered cavity magnomechanics, Phys. Rev. A **103**, 063708 (2021).

[85] M. Braun, *Differential Equations and Their Applications*, 3rd ed. (Springer, New York, 1983).

[86] E. X. DeJesus and C. Kaufman, Routh-Hurwitz criterion in the examination of eigenvalues of a system of nonlinear ordinary differential equations, Phys. Rev. A **35**, 5288 (1987).

[87] C. Dembowski, H.-D. Gräf, H. L. Harney, A. Heine, W. D. Heiss, H. Rehfeld, and A. Richter, Experimental Observation of the Topological Structure of Exceptional Points, Phys. Rev. Lett. **86**, 787 (2001).

[88] A. Regensburger, C. Bersch, M.-A. Miri, G. Onishchukov, D. N. Christodoulides, and U. Peschel, Parity-time synthetic photonic lattices, Nature (London) **488**, 167 (2012).

[89] C. E. Rüter, K. G. Makris, R. El-Ganainy, D. N. Christodoulides, M. Segev and D. Kip, Observation of parity-time symmetry in optics, Nat. Phys. **6**, 192 (2010).

[90] F. Klauck, L. Teuber, M. Ornigotti, M. Heinrich, S. Scheel and A. Szameit, Observation of $\mathcal{PT}$-symmetric quantum interference, Nat. Photonics **13**, 883 (2019).

[91] I. Mahboob, K. Nishiguchi, H. Okamoto, and H. Yamaguchi, Coherent phonon manipulation in coupled mechanical resonators, Nat. Phys. **8**, 387 (2012).

[92] K. V. Kepesidis, S. D. Bennett, S. Portolan, M. D. Lukin, and P. Rabl, Phonon cooling and lasing with nitrogen-vacancy centers in diamond, Phys. Rev. B **88**, 064105 (2013).

[93] J.-H. Kim, M. C. Kuzyk, K. Han, H. Wang, and G. Bahl, Non-reciprocal Brillouin scattering induced transparency, Nat. Phys. **11**, 275 (2015).